Langmuir

Subscriber access provided by INDIAN INST OF TECH MADRAS

Research Article

Interaction of Azide Ion with Hemin and Cytochrome *c* Immobilized on Au and Ag Nanoparticles

Renjis T. Tom, and T. Pradeep

Langmuir, **2005**, 21 (25), 11896-11902• DOI: 10.1021/la052035o • Publication Date (Web): 02 November 2005

Downloaded from http://pubs.acs.org on February 17, 2009

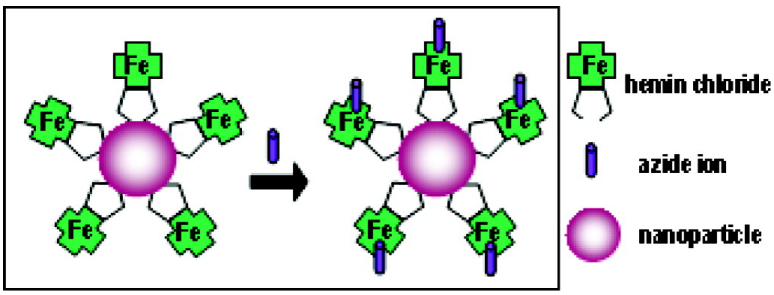

More About This Article

Additional resources and features associated with this article are available within the HTML version:

- Supporting Information
- Links to the 4 articles that cite this article, as of the time of this article download
- Access to high resolution figures
- Links to articles and content related to this article
- Copyright permission to reproduce figures and/or text from this article

View the Full Text HTML

ACS Publications
High quality. High impact.

Langmuir is published by the American Chemical Society. 1155 Sixteenth Street N.W., Washington, DC 20036

Interaction of Azide Ion with Hemin and Cytochrome *c* Immobilized on Au and Ag Nanoparticles

Renjis T. Tom and T. Pradeep*

DST Unit on Nanoscience, Department of Chemistry and Sophisticated Analytical Instrument Facility, Indian Institute of Technology Madras, Chennai 600 036, India

Received July 27, 2005. In Final Form: September 22, 2005

This paper presents a set of investigations on the binding of a metabolic inhibitor, azide with prosthetic heme group of biomolecules, hemin chloride (Hem) and cytochrome *c* (Cyt *c*) immobilized on Au and Ag nanoparticles. A variety of spectroscopic tools have been used to understand the chemistry occurring on the nanoparticle surface. While the nature of binding of the model system, hemin has been investigated by UV−visible, fluorescence, FTIR, and Raman spectroscopies, the azide binding has been studied in detail by MALDI-TOF MS. Hemin binding on the nanoparticle surface occurs through the carboxylic acid groups. The hemin−N_3 adduct on the nanoparticle surface has been detected by mass spectrometry and its fragments have been studied by post source decay analysis. The chemistry of hemin on the nanoparticle surface has been compared with that of the protein, Cyt *c*. Azide binding of Cyt *c* requires thermal activation due to reduced accessibility of the heme center, unlike in the case of hemin. The binding chemistry is similar for free Cyt *c* and Cyt *c* bound to the nanoparticles.

Introduction

Self-organization of molecules is one of the fundamental aspects of all biological systems. Self-organization of nanometer sized biomolecules leads to micron sized living cells. To study the intercellular and intracellular biological processes, there is a necessity of probes in the nanometer dimension, which are now available in the form of nano−bio hybrid systems. Nanoparticles in the size regime of 1−100 nm are approximately 100−10,000 times smaller than human cells. They are comparable in size to bulky biological molecules such as proteins. For instance, hemoglobin, the oxygen carrier in red blood cells, is around 5 nm in diameter. Metal nanoparticles are ideal candidates for synthesizing hybrid nano-bio assemblies because of their natural size compatibility. The initial steps on this track leading to a rational approach of hybrid nano-bio assembly were made by the groups of Mirkin[1] and Alivisatos,[2] who demonstrated that DNA-modified nanoparticles could be assembled into superstructures by hybridization of complementary base sequences of the surface-bound DNA molecules. The interaction of a specific molecule with a protein receptor in a biological recognition process is often related to an alteration in the protein conformation as a response to the binding event. Design and development of target-molecule-recognizing hybrid nano−bio assemblies that can account for such changes via signal transduction in a medium are of interest to many scientists.[3]

The electronic absorption spectra of nanoparticles are highly sensitive to changes in the dielectric constant of the neighboring microenvironment, and these optical properties can be utilized for the detection of specific biomolecules.[4] Nano−bio hybrid systems are capable of detecting target molecules from biological fluids at extremely low concentrations.[5,6] Enzymes immobilized on gold nanoparticle surfaces are found to be active to perform reactions in organic media.[7] The 15 nm sized gold nanoparticles have been used as diagnostic probes for antibodies, which are the markers of diseases.[8] The detection of cancer biomarker proteins in biological fluids is extremely difficult, for their concentration level is between nano and pico moles.[9] A recent analytical methodology utilized nanoparticles as preconcentration probes for proteins in biological fluids at extremely low concentrations.[10,11]

Scheme 1. Molecular Structure of Hemin Chloride (Hem)

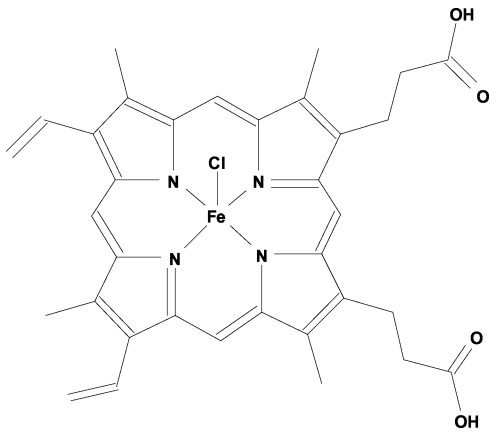

We used hemin chloride (Hem, Scheme 1) and cytochrome *c* (Cyt *c*) in our studies. Hemin is a protoporphyrin

* To whom correspondence should be addressed. E-mail: pradeep@iitm.ac.in. Fax: 044-2257 0545/0509.

(1) Mirkin, C. A.; Letsinger, R. L.; Mucic, R. C.; Storhoff, J. J. *Nature* **1996**, *382*, 607−608.
(2) Alivisatos, A. P.; Johnsson, K. P.; Peng, X. G.; Wilson, T. E.; Loweth, C. G.; Bruchez, M. P.; Schultz, P. G. *Nature* **1996**, *382*, 609−611.
(3) Rosi, N. L.; Mirkin, C. A. *Chem. Rev.* **2005**, *105*, 1547−1562.
(4) Aslan, K.; Lakowicz, J. R.; Geddes, C. D. *Anal. Biochem.* **2004**, *330*, 145−155.
(5) Cheng, S.-F.; Chau, L.-K. *Anal. Chem.* **2003**, *75*, 16−21.
(6) Nath, N.; Chilkoti, A. *Anal. Chem.* **2002**, *74*, 504−509.
(7) Phadthare, S.; Vinod, V. P.; Mukhopadhyay, K.; Kumar, A.; Rao, M.; Chaudhari, R. V.; Sastry, M. *Biotechnol. Bioeng.* **2004**, *85*, 629−637.
(8) Xu, W.; Xu, S.; Ji, X.; Song, B.; Yuan, H.; Ma, L.; Bai, Y. *Colloids Surf. B: Biointerfaces* **2005**, *40*, 169−172.
(9) Neih, S.; Chen, S.-F.; Chu, T.-Y.; Lai, H.-C.; Fu, E. *Gynecol. Oncol.* **2003**, *91*, 201−208.
(10) Teng, C.-H.; Ho, K.-C.; Lin, Y.-S.; Chen, Y.-C. *Anal. Chem.* **2004**, *76*, 4337−4342.
(11) Ho, K.-C.; Tsai, P.-J.; Lin, Y.-S.; Chen, Y.-C. *Anal. Chem.* **2004**, *76*, 7162−7168.

10.1021/la052035o CCC: $30.25 © 2005 American Chemical Society
Published on Web 11/02/2005

IX Fe (III) complex, which is the active part of hemoglobin.[12] Cyt *c* is an electron transport agent in mitochondria.[13] Heme is a prosthetic group present in a large number of biomolecules in living systems performing key biological functions such as oxygen transport, electron transport, and many redox processes. Selective inhibition of the biological activity of heme is a central issue for the development of many antifungal drugs. In the normal strategy, either synthetic derivatives of imidazole[14−16] or 1,2,4-triazole[17] bind to the Fe (III) center of the prosthetic heme group, arresting its metabolic activity.

We used Ag and Au nanoparticles as templates to construct a nanosized assembly of biomolecules. We note that, in order to understand the mechanism of metabolic activity of the heme moiety, gaseous ligands such as carbon monoxide and nitric oxide[18] are often used. The binding of anionic ligands such as cyanide,[19] fluoride,[19] and azide[19,20] to Fe (III) center of free hemoprotiens was investigated by electronic and vibrational spectroscopies. The early reports of Cyt *c* immobilization on Au and Ag nanoparticles were by Natan et al., who studied the resultant bioconjugates by surface enhanced Raman spectroscopy.[21,22] The retention of conformations under pH fluctuations has been observed in the case of Au and Ag nanoparticle-immobilized Cyt *c*.[23,24] Cyt *c* immobilized Au nanoparticles have been incorporated into a silica gel matrix[25] and the resultant material showed sensing of nitric oxide. The conformational alterations of bovine heart cytochrome *c* caused by the immobilization on gold nanoparticle surface as a function of particle size have been reported.[26] We chose azide ion as a heme binding ligand because of its aqueous phase reactivity,[27] simple molecular structure, and the occurrence of a strong absorption feature in the infrared spectrum. We undertook this research as part of our ongoing studies on the self-organization of mercaptans, antibiotics, and fatty acids on noble metal nanoparticles[28−30] and core−shell nanoparticles.[31−32]

Experimental Section

Materials. Hemin chloride (bovine) and sodium borohydride were purchased from Sigma Aldrich. Tetrachloroauric acid trihydrate ($HAuCl_4 \cdot 3H_2O$), silver nitrate ($AgNO_3$), sodium citrate, and sodium azide (NaN_3) were purchased from CDH. Ferric cytochrome *c* (horse heart) was purchased from Sisco Research Laboratories, India. Ethanol was purchased from Tedia Company, U.S.A. All chemicals were used as such without further purification. Triply distilled deionized water was used for all of the experiments. Potassium bromide (spectroscopic grade), used for infrared studies, was purchased from Merck. Sinapinic acid was used as the matrix for matrix assisted laser desorption ionization−time-of-flight mass spectrometry (MALDI-TOF MS).

Synthesis of Hem Capped Au and Ag Nanoparticles. Citrate capped gold, Au(15 nm)@Cit[33] and silver Ag(4 nm)@Cit[34] and Ag(60 nm)@Cit[33] nanoparticles were synthesized according to reported procedures. These will be referred to below as Au, Ag(I), and Ag(II) particles, respectively. The nanoparticle solution (80 mL) was mixed with 20 mL of 0.02 mg/mL Hem in 20% aqueous ethanol. The sample was stirred for 72 h and allowed to settle for 24 h. The precipitate was centrifuged at 2500 rpm and washed three times with 10% aqueous ethanol to remove unbound Hem. Hem capped silver (Ag@Hem) and gold (Au@Hem) nanoparticles were characterized by UV−visible spectroscopy, FTIR spectroscopy, confocal Raman spectroscopy, and laser desorption ionization−time-of-flight mass spectrometry (LDI-TOF MS).

Synthesis of Azide Complex of Au@Hem and Ag@Hem. A mixture of 20 mL of 2.0 mg/mL Au@Hem or Ag@Hem and 5 mL of 0.65 mg/mL sodium azide, in 20% aqueous ethanol was allowed to stir for 24 h and kept undisturbed for 12 h. The precipitate was centrifuged at 2500 rpm and washed three times with 10% aqueous ethanol to remove unbound azide. Au@Hem-N_3 or Ag@Hem-N_3 formed was characterized by FTIR spectroscopy and LDI-TOF MS.

Synthesis of Cyt *c* Capped Au and Ag Nanoparticles. A mixture of 5 mL of 1.0 mg/mL Cyt *c* in water and 20 mL of Au, Ag (I), or Ag (II) nanoparticles was stirred gently at room temperature for 24 h. The resultant solution was kept undisturbed for 12 h and was centrifuged at 2500 rpm for 20 min. The precipitate was washed with ice cold water to remove ionic impurities. The purple (Au@Cyt *c*) or reddish brown (Ag@Cyt *c*) residue was analyzed by UV−visible spectroscopy, FT-IR spectroscopy, fluorescence spectroscopy, and MALDI -TOF MS.

Synthesis of Azide Complex of Au@Cyt *c* and Ag@Cyt *c*. The Au@Cyt *c* or Ag@Cyt *c* 2.0 mg/mL was dispersed in 20 mL of 0.65 mg/mL NaN_3 containing aqueous phosphate buffered saline (PBS) at pH 7.2, and the mixture was stirred gently for 24 h. The resultant solution was kept undisturbed for 12 h and was centrifuged at 2500 rpm for 20 min. The sample was washed three times with ice cold water in order to remove the free azide.

Synthesis of Azide Bound Nanoparticles. A mixture of 20 mL of Au, Ag(I), or Ag (II) and 5 mL of 0.65 mg/mL sodium azide was stirred for 72 h and kept undisturbed for 24 h. The aggregated azide capped nanoparticles (Au@N_3 and Ag@N_3) were separated by centrifugation. The samples were washed three times with ice cold water in order to remove free azide and were analyzed by UV−visible spectroscopy and FTIR spectroscopy.

Reaction of Azide with Cyt *c*. A total of 20 mL of 0.2 mg/mL Cyt *c* was prepared in 0.65 mg/mL NaN_3 containing phosphate buffered saline (PBS). The sample was divided into four portions of equal volume. Each portion was maintained at a particular temperature for 60 min using a water bath, and the complex was separated by centrifugation and washed three times with ice cold water in order to remove free azide. A control experiment was done without the azide ion in which 20 mL of 1 mg/mL Cyt *c* was prepared in phosphate buffered saline (PBS), divided into

(12) Yang, W.; Zheng, H.; Yuan, W.-T.; Xu, J.-G. *Anal. Sci.* **2004**, *20*, 1265−1270.
(13) Yang, J.; Liu, X.; Bhalla, K.; Kim, C. N.; Ibrado, A. M.; Cai, J.; Peing, T.-I.; Jones, D. P.; Wang, X. *Science* **1997**, *275*, 1129−1132.
(14) Zhang, X.; Yu, R. M. K.; Jones, P. D.; Lam, G. K. W.; Newsted, J. L.; Gracia, T.; Hecker, M.; Hilscherova, K.; Sanderson, J. T.; Wu, R. S. S.; Giesy, J. P. *Environ. Sci. Technol.* **2005**, *39*, 2777−2785.
(15) Chen, Z.; Wang, L.-H.; Shelvis, J. P. M. *Biochemistry* **2003**, *42*, 2542−2551.
(16) Lepesheva, G. I.; Virus, C.; Waterman, M. R. *Biochemistry* **2003**, *42*, 9091−9101.
(17) Mastumoto, M.; Ishida, K.; Konagai, A.; Maebashi, K.; Asaoka, T. *Antimicrob. Agents Chemother.* **2002**, *46*, 308−314.
(18) Andrew, C. R.; Green, E. L.; Lawson, D. M.; Eady, R. R. *Biochemistry* **2001**, *40*, 4115−4122.
(19) Viola, F.; Aime, S.; Coletta, M.; Desideri, A.; Fassano, M.; Paoletti, S.; Tarricone, C.; Ascenzi, P. *J. Inorg. Biochem.* **1996**, *35*, 213−222.
(20) Yoshikawa, S.; Caughey, W. S. *J. Biol. Chem.* **1992**, *267*, 9757−9766.
(21) Keating, C. D.; Kovaleski, K. M.; Natan, M. J. *J. Phys. Chem. B* **1998**, *102*, 9404−9413.
(22) Keating, C. D.; Kovaleski, K. M.; Natan, M. J. *J. Phys. Chem. B* **1998**, *102*, 9414−9425.
(23) Wallace, J. M.; Rice, J. K.; Pietron, J. J.; Stroud, R. M.; Long, J. W.; Rolison, D. R. *Nano Lett.* **2003**, *3*, 1463−1467.
(24) Wallace, J. M.; Dening, B. M.; Eden, K. B.; Stoud, R. M.; Long, J. W.; Rolison, D. R. *Langmuir* **2004**, *20*, 9276−9281.
(25) Wallace, J. M.; Stroud, R. M.; Pietron, J. J.; Long, J. W.; Rolison, D. R. *J. Non-Cryst. Solids* **2004**, *350*, 31−38.
(26) Jiang, X.; Jiang, J.; Jin, Y.; Wang, E.; Dong, S. *Biomacromolecules* **2005**, *6*, 46−53.
(27) Manabe, T.; Manabe, N.; Hiromi, K.; Hatano, H. *FEBS Lett.* **1971**, *16*, 201−203.
(28) Pradeep, T.; Mitra, S.; Nair, A. S.; Mukhopadhyay, R. *J. Phys. Chem. B* **2004**, *108*, 7012−7020.
(29) Sandhyarani, N.; Pradeep, T. *Int. Rev. Phys. Chem.* **2003**, *22*, 221−262.
(30) Tom, R. T.; Suryanarayanan, V.; Reddy, P. G.; Baskaran, S.; Pradeep, T. *Langmuir* **2004**, *20*, 1909−1914.
(31) Tom, R. T.; Nair, A. S.; Singh, N.; Aslam, M.; Nagendra, C. L.; Philip, R.; Vijayamohanan, K.; Pradeep, T. *Langmuir* **2003**, *19*, 3439−3445.
(32) Nair, A. S.; Pradeep, T.; MacLaren, I. *J. Mater. Chem.* **2004**, *14*, 857−862.
(33) Turkevich, J.; Stevenson, P. C.; Hillier, J. *Discuss. Farady Soc.* **1951**, *11*, 55−75.
(34) Obrae, S. O.; Rachael, E.; Hollowell, R. E.; Murphy, C. J. *Langmuir* **2002**, *18*, 10407−10410.

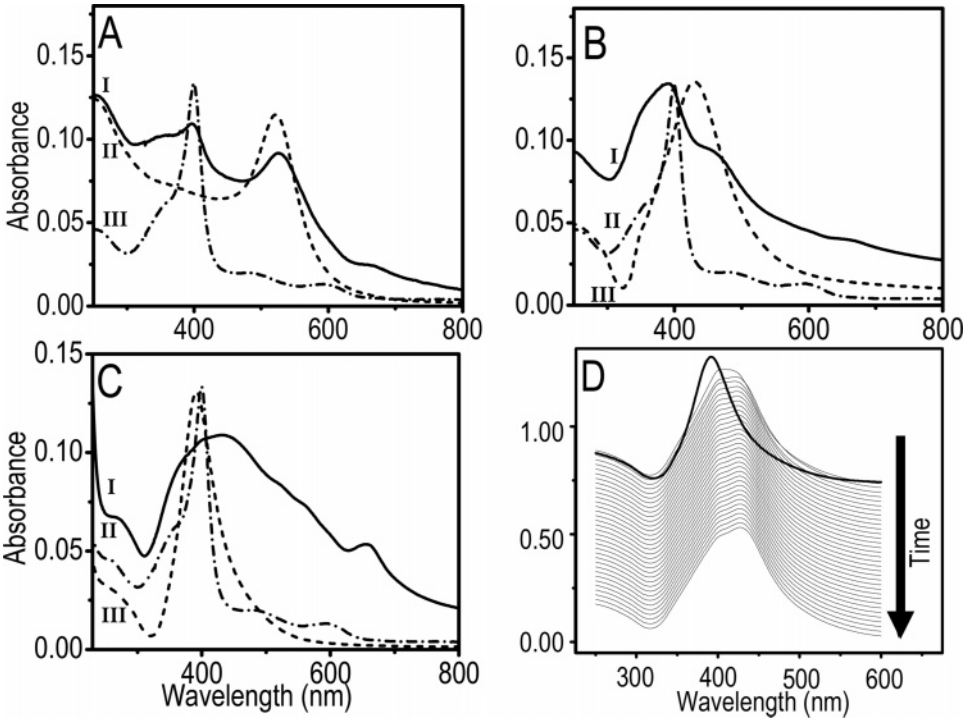

Figure 1. (A−C) UV−visible spectra of Au, Ag (II), and Ag (I) particles, respectively taken in 20% aqueous ethanol. Traces (I), (II), and (III) represent the Hem capped nanoparticles, M@Hem, citrate capped nanoparticles, M@Cit and 0.004 mg/mL hemin chloride, respectively. (D) Time dependent binding of Hem on Ag (4 nm) particle monitored at a time interval of 10 min for the initial 6 h. Thick curve in D corresponds to the parent nanoparticle solution.

four equal portions, maintained at a particular temperature for 60 min, and analyzed using UV−visible and FTIR spectroscopies.

Temperature-Dependent Transformations of Au@Cyt *c*-N_3. A total of 20 mL of 2 mg/mL Au@Cyt *c*-N_3 was prepared in phosphate buffered saline (PBS). The sample was divided into four portions of equal volume. Each portion was maintained at a particular temperature for 30 min using a water bath, and the complex was separated by centrifugation and washed three times with ice cold water in order to remove free azide. Investigations were done with UV−visible and FTIR spectroscopies.

Instrumentation. UV−visible spectra were measured using a Perkin-Elmer Lambda 25 spectrometer. Fluorescence spectra were measured using JOBIN−YVON Fluorolog model spectrometer in aqueous medium. Transmission electron microscopy was performed using a Philips CM12 transmission electron microscope (TEM) operating at 120 keV. The samples for TEM were prepared by dropping the dispersion on copper-grid-supported Formvar films. For recording infrared spectra, vacuum-dried samples were made in the form of 1% (by weight) KBr pellets and the spectra were measured with a Perkin-Elmer Spectrum One FT-IR spectrometer. Raman spectra were measured using a Confocal Raman spectrometer CRM 200 of Witec. Mass spectrometric studies were conducted using a Voyager DE PRO Biospectrometry Workstation of Applied Biosystems MALDI-TOF MS. A pulsed nitrogen laser of 337 nm was used (maximum firing rate, 20 Hz; maximum pulse energy, 300 μJ) for MALDI-TOF−MS studies. Mass spectra were collected in positive and negative ion modes and were averaged for 100 shots. Post source decay (PSD) spectra were measured using the reflectron analyzer, in the positive mode.

Results and Discussion

The UV− visible spectra presented in Figure 1 illustrate the effect of binding of Hem on nanoparticles: Au, Ag (I), and Ag (II). Both the Ag nanoparticles showed more aggregation tendency after binding to Hem as compared to Au. The reason for the more aggregated nature of Ag nanoparticles after Hem binding is attributed to the presence of carboxy groups in hemin which are known to bind to Ag surfaces. They may also be involved in the interlinking of nanoparticles. This is manifested in the absorption spectra. Although the plasmon of Au nanoparticle is distinctly evident in (A) even after Hem binding, Ag (I) particles show the signature of aggregation, resulting in a broad feature (C). The Ag (II) particles show the plasmon feature clearly even after binding, but aggregation is, however, evident from the increase in the background intensity at 800 nm (B). The peak maximum of the plasmon band is apparently shifted to lower and higher values in the case of Ag (II) and Ag (I) particles, respectively. Both blue shifts and red shifts as a result of an increase in size of nanoparticles have been reported, and in the quasistatic regime, the nature of shifts is influenced by several factors.[35]

The number of Hem molecule per nanoparticle is calculated from the Soret band intensity of Hem (Supporting Information). There are 23, 245, and 4608 molecules capping the nanoparticles, Ag (I), Au, and Ag (II), respectively. The areas occupied by a single Hem molecule on the surface are 2.18, 2.90, and 2.45 nm^2 for Ag (I), Au, and Ag (II) particles, respectively. Although the area on Ag is around 2.3 nm^2, that on Au is substantially higher. The larger packing density on Ag may be attributed to increased affinity of the −COOH groups to the metal surface (see below).

In the case of Au@Hem (Figure 1A), we can see the Soret band of Hem at 400 nm[12,36] but those of Ag (II)@Hem (Figure 1B) and Ag (I)@Hem (Figure 1C) are overlapped with the surface plasmon resonance (SPR) band of the aggregated silver clusters. Aggregation can also be visualized by the naked eye in the form of a color change after Hem binding. There is a color change from wine red to purple, deep yellow to yellowish green, and yellowish

(35) Link, S.; El-Sayed, M. A. *J. Phys. Chem. B* **1999**, *103*, 8410−8426.

(36) Wood, B. R.; Langford, S. J.; Cooke, B. M.; Lim, J.; Glenister, F. K.; Duriska, M.; Unthank, J. K.; McNaughton, D. *J. Am. Chem. Soc.* **2004**, *126*, 9233−9239.

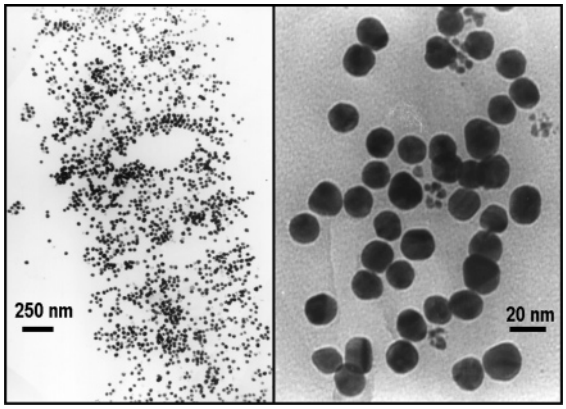

Figure 2. Transmission electron micrograph of Hem capped gold nanoparticles (Au@Hem). The left side image is of large area, indicating well separated nanoparticles. In the right side image (small area), the 15 nm particles are seen.

green to greenish brown for Au, Ag (I), and Ag (II) particles, respectively. Traces (II) in all panels represent the SPR band of citrate capped nanoparticles. The Au, Ag (II), and Ag (I) particles show strong SPR band at 520 (Figure 1A), 430 (Figure 1B), and 392 nm (Figure 1C), respectively. Binding of Hem on the surface of metal nanoparticles is a slow process, which takes 3 days to complete. Figure 1D represents the time dependent monitoring of the process for the initial hours. Each trace is taken at an interval of 10 min. The slow formation of aggregates of Ag (I) nanoparticles as a function of time can be inferred from the changes in the shape of the SPR band. The dispersion of Au@Hem is stable for 3 months in 20% aqueous ethanol. Ag nanoparticles show aggregated structures after Hem binding.

In Figure 2, TEM images of Au@Hem are shown. We see well separated nanoparticles, agreeing with the UV−vis observation. The enlarged image shows 15 nm particles.

The vibrational spectra of the systems can be better understood considering the structure. It consists of a protoporphyrin (IX) ring system, and Fe (III) occupies the center of its cavity, with a coordinated chloride ion (Scheme 1). The Fe (III) center is square pyramidal in geometry, due to the penta coordination of ligands. The ring has side chain carboxy ethyl, vinyl, and methyl groups. The infrared spectrum (Figure 3) in the fingerprint region of Hem (panel A) shows a sharp band at 1700 cm^{-1}, which corresponds to the C=O stretch of the carboxylic acid groups. After binding to the metal nanoparticle surfaces, the band splits into two (1664 and 1713 cm^{-1}) in all of the cases. The peaks observed at 1664 and 1713 cm^{-1} correspond to the C=O stretch of surface bound carboxyl group and of hydrogen bonded free carboxylic acid group,[36] respectively. The enhanced band observed at 1209 cm^{-1} is due to the C−O stretching vibration of the surface bound carboxyl group,[36] which is observed in samples B−D. This indicates that the Hem molecule is bound to the nanoparticle surface through the carboxylic acid linkage. Another small peak is observed at 1630 cm^{-1}, due to the $\nu_{10}(C_\alpha-C_\beta)$ band of the porphyrin skeleton.[36] This Raman active mode appear better in the case of Ag (I) particles (D), possibly due to the increased structural distortion of the molecule on a smaller nanoparticle surface. To understand more about the Hem monolayer on the nanoparticle surface, we studied the Raman spectra of all of the samples mentioned above.

The Raman spectrum of Hem (A) shows major bands at 1609, 1539, and 1341 cm^{-1} which correspond to the asymmetric C−C stretching, $\nu_{10}(C_\alpha-C_m)_{asym}$; asymmetric

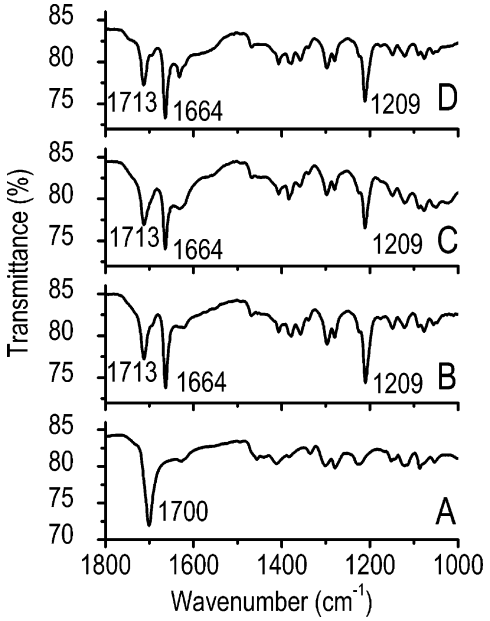

Figure 3. FTIR spectra of Hem (A), Au@Hem (B), Ag(II)@Hem (C), and Ag(I)@Hem (D), recorded in KBr matrix.

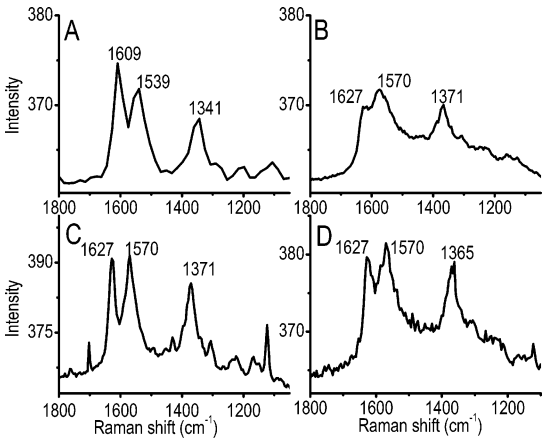

Figure 4. Raman spectra of Hem (A), Au@Hem (B), Ag(II)@Hem (C), and Ag(I)@Hem (D), recorded using 514 nm laser excitation through a confocal (60 ×) objective.

C−C stretching, $\nu_2(C_\beta-C_\beta)_{asym}$; and symmetric pyrrole-half-ring stretching, $\nu_4(\text{Pyr half-ring})_{sym}$ of the protoporphyrin (IX) ring system.[12,36,37] After binding to the metal nanoparticles, $\nu_{10}(C_\alpha-C_m)_{asym}$, $\nu_2(C_\beta-C_\beta)_{asym}$, and $\nu_4(\text{Pyr half-ring})_{sym}$ are shifted to 1627, 1570, and 1371 cm^{-1}, respectively.[12,36,37] Enhancement of the Raman signal at 1570 and 1371 cm^{-1} is observed in the case of all of the nanoparticle bound samples, B−D. The surface enhancement of the Raman signal is highest in the case of Ag (II) particles and lowest in the case of Au particles. Hardening of the Raman modes after binding is an indication of the confinement of the molecule on the nanoparticle surface. The binding of Hem is similar on all surfaces as suggested by the corresponding Raman features. From both FTIR and Raman data, it is clear that the Hem molecule binds to both Au and Ag surfaces through the carboxyl group and there is a confinement of Hem molecule above the nanoparticle surface.

Figure 5 presents LDI-TOF mass spectra of Hem containing samples before and after the reaction with azide. The molecular ion peak at m/z = 651 has the

(37) Schlucker, S.; Koster, J.; Nissum, M.; Popp, J.; Keifer, W. *J. Phys. Chem. A* **2001**, *105*, 9482−9488.

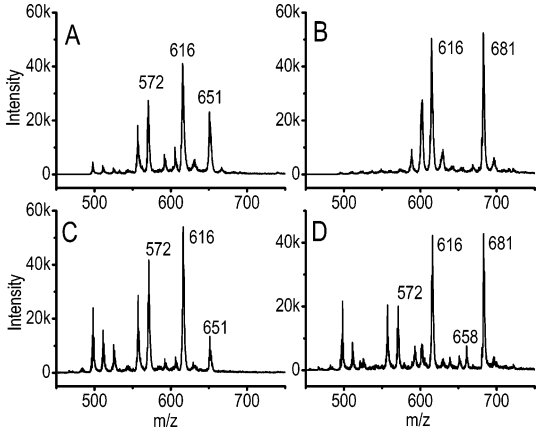

Figure 5. LDI−TOF mass spectra recorded in the positive ion mode for Hem (A), Hem-azide complex (B), Au@Hem (C), and Au@Hem-N_3 (D).

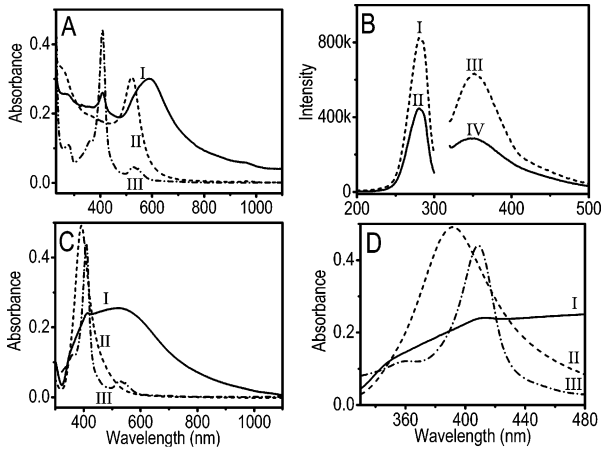

Figure 6. (A and B) Absorption and emission spectra, respectively of the Au@Cyc system. Traces (I), (II), and (III) of A correspond to 0.2 mg/mL Au@Cyt *c*, 0.1 mg/mL Au@Cit and 0.1 mg/mL Cyt *c*, respectively. (B) Excitation and emission spectra of [(I) and (III)] free Cyt *c* (0.01 mg/mL) and [(II) and (IV)] Au@Cyt *c* (0.05 mg/mL) taken in water. C is the absorption data of the Ag(I) nanoparticle system. The traces (I), (II), and (III) have correspond to similar systems as in A. (D) An enlarged view of panel C in the region, 350−480 nm.

characteristic isotopic pattern of chlorine. The peak at *m/z* = 616 is the daughter ion formed due to Cl^- loss. The mass peak at *m/z* = 572 corresponds to the daughter ion formed by CO_2 loss. The spectrum of Au@Hem (panel B) is similar to Hem (panel A) itself. After reaction with azide, the peak at *m/z* 651 disappeared completely indicating that N_3^- is completely substituting Cl^- from the Fe (III) center. The reaction can be proposed as

$$\text{Hem-Cl} + N_3^- \rightarrow \text{Hem-}N_3 + Cl^-$$

$$\text{Au@Hem-Cl} + N_3^- \rightarrow \text{Au@Hem-}N_3 + Cl^- \text{ or}$$

$$\text{Ag@Hem-Cl} + N_3^- \rightarrow \text{Ag@Hem-}N_3 + Cl^-$$

The molecular ion peak of the azide complex appears at *m/z* = 681, which corresponds to Hem + $^{14}N_3$ + ^{23}Na and its daughter ion at *m/z* = 658 is due to Hem + $^{14}N_3$. The LDI-TOF mass spectrum of Ag@Hem-N_3 is similar to that of Hem-N_3, although there is difference in relative intensities (Supporting Information). The nanoparticle samples show the Ag ion peak as a doublet at *m/z* = 107 and 109. The formation of daughter ions by fragmentation was confirmed by post source decay analysis. PSD analysis of the peak at *m/z* = 616 (Hem) shows peaks at *m/z* = 572, 556, and 543. PSD analysis of *m/z* = 651 (Hem-Cl) shows peaks at *m/z* = 616, 591, and 572. PSD is not the best fragmentation mode and therefore, an ideal daughter ion spectrum is not obtained. However, generation of certain daughter ions from the molecular ions is established (Supporting Information).

Having studied the model system Hem, we went on to investigate the protein, Cyt c. In contrast to the earlier reports which were focused on the conformational stability and the nature of interaction of the Cyt *c* molecule on Au and Ag nanoparticle surfaces, in this study, we concentrated on the chemical accessibility of the heme unit of the nanoparticle bound Cyt *c* and compared it with the free molecule. As binding of Cyt *c* on nanoparticles has been investigated before,[24−26] we present only the essential and newer aspects here. In Figure 6, we present the optical spectroscopic data of M@Cyt *c*. In Figure 6A, trace (II) represents citrate capped gold nanoparticles (Au@Cit), showing a sharp SPR band at 520 nm. Trace (III) shows a strong Soret band at 408 nm and a weak Q-band at 540 nm, due to the electronic excitation of the heme unit of the Cyt *c*.[26] The formation of Au@Cyt *c* is clearly visible from the color change from wine red to purple. Absence of nanoparticle aggregation in this sample is due to electrostatic repulsion between thicker Cyt *c* shells of neighboring nanoparticles.[26] Trace (I) shows the Soret band at 408 nm and a broadened SPR band at 590 nm. Due to the changes in dielectric constant of the neighboring environment,[26] the SPR band of Au@Cyt *c* is broadened and red-shifted by 70 nm. In Figure 6C, trace (II) is citrate capped silver nanoparticle, Ag (I) showing a sharp SPR band at 392 nm. The formation of Ag@Cyt *c* is clearly visible from the color change from yellow to reddish brown. The trace (I) shows a Soret band at 408 nm and a broadened SPR band at 523 nm. Due to the change in the dielectric constant of the neighboring environment[26] of the silver nanocore, the SPR band of Ag@Cyt *c* is broadened and red-shifted. Figure 6D shows an enlarged view, showing clearly the Soret band of Cyt *c* and SPR band of Ag (I) nanoparticles.

Figure 6B shows the fluorescence spectra taken in aqueous medium. The emission maxima for both Cyt *c* (III) and Au@Cyt *c* (IV) are at 352 nm. The number of Cyt *c* molecules present in both samples is the same. The excitation spectrum shows the same peak position in both the samples. The absence of a shift in the emission and excitation of Au@Cyt *c* compared to free Cyt *c* indicates that the fluorophore, tryptophan moiety is away from the surface of the nanoparticle. The decreased fluorescence confirms that some of the excited fluorophore are quenched by the gold nanocore.[30] The experiment carried out with Ag (II)@Cyt *c* and Ag (II)@Cyt *c*-N_3 showed that the reduction in intensity is less, in comparison to Au (Supporting Information). We note that enhancement of fluorescence intensity by silver nanostructures has been reported by Lackowicz and colleagues for proteins such as human serum albumin at very low concentration.[38,39] We believe that such enhancement is not seen in this system probably due to multilayer coverage of Cyt *c* and its inherently reduced fluorescence intensity due to the presence of the heme unit close to the fluorophore. Rolison et al. used fluorescence spectroscopy to study conformational stability of immobilized Cyt *c* molecules under various pH conditions.[23,24]

(38) Aslan, K.; Leonenko, Z.; Lakowicz, J. R.; Geddes, C. D. *J. Phys. Chem. B* **2005**, *109*, 3157−3162.
(39) Aslan, K.; Lakowicz, J. R.; Geddes, C. D. *J. Phys. Chem. B* **2005**, *109*, 6247−6251.

The intensity of the Soret band at 408 nm of Cyt *c* which remained in the mother liquor after complete removal of M@Cyt *c* by centrifugation, was used for calculating the number of molecules per nanoparticle. It was found that 3 and 4 shells of Cyt *c* molecules were sitting around Au (15 nm) and Ag (4 nm) particle, respectively.[24] The number of molecules per nanoparticle is 700 and 55 for Au and Ag (4 nm) particles, respectively. Transmission electron micrograph shows well separated uniform sized nanoparticles (15 nm) (Supporting Information). The samples, Au@Cyt *c* and Ag@Cyt *c*, were analyzed by MALDI-TOF MS. The mass spectra showed a peak at *m/z* 12574 for both samples, in the positive and negative ion modes. This *m/z* value is similar to that of the mass spectrum of pure Cyt *c*.[10] The MALDI-TOF MS analysis of Au@Cyt *c* confirms that Cyt *c* is capping the gold nanoparticles (Supporting Information).

Figure 7, panels A and C, presents the reaction of azide with free Cyt *c*, at different temperatures in aqueous PBS. There is no significant change in the Soret band when the sample was kept at 30 °C. The *Q* band showed a marginal change. Altogether, the extent of reaction at room temperature is insignificant. However, both the bands changed when the sample was heated at 50 °C. This indicates the occurrence of a reaction. The Soret band has shifted from 408 to 412 nm for the samples heated above 50 °C. There is an observable change in the *Q* band also. Two well-defined bands appeared at 521 and 549 nm. Panels B and D of Figure 7 represent the Soret band and the *Q* band, respectively, of the control experiment carried out under identical conditions without the azide ion. No characteristic change is observed for the Soret band. The Q-band changes slightly due to an increase in the background, but the distinct features as seen in C are absent. Thus, from the control experiment, it is clear that the changes observed in the UV−visible features of Cyt *c* are due to the complexation and not due to thermally induced conformational changes.

To understand the mechanism of the azide binding to the hemoproteins, the bis(1-methyl imidazole) ferric heme complexes were taken as model systems.[40] From the reports, it is clear that azide is replacing one of the imidazole groups and one of the terminal nitrogen of azide ion is binding to the Fe (III) center.[41] The changes occurring in both these bands above 30 °C are due to the complexation of azide by substituting the imidazole ligand. The reaction is not happening at 30 °C because thermal activation is required for the azide ion to substitute the imidazole ligand, which is part of the histidine moiety of the protein structure. The conformational rigidity of the protein does not allow the reaction to occur at room temperature. Thermal activation of azide ion binding has not been investigated before.

Further insight into the azide binding is obtained from the infrared spectra (Figure 8). Azide binding was investigated with gold (15 nm) and silver (4 and 60 nm) (data not shown) nanoparticles. Asymmetric stretching ν_{as} (N_3) of the free azide is observed at 2036 cm^{-1} in the FTIR spectrum.[42] This feature is observed in the (a) traces of both Au@Hem-N_3 (A) and Au@Cyt-N_3 (B) due to the presence of azide ion bound to the surface of the nanoparticle, through electrostatic interactions. This observation is confirmed from trace (c) which corresponds to Au@N_3. The shoulders observed in traces (a) of Figure 8, panels A and B, near 2057 and 2047 cm^{-1} are due to the azide ion bound to Fe (III) center[43] of Hem and Cyt *c*, respectively. The traces (d) of Figure 8, panels A and B, correspond to Au@Hem and Au@Cyt *c*, respectively, which do not show any characteristic feature in the above region.

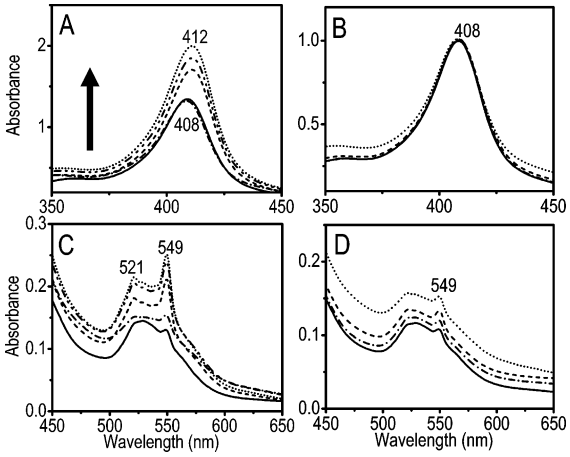

Figure 7. UV-visible spectra of Cyt *c* in phosphate buffered saline as a function of temperature. Panels A and C represent the Soret band and *Q* band of Cyt *c*, respectively. The solid line represents the UV−visible spectrum at room temperature. The other traces represent the UV−visible spectra of Cyt *c* reacted with azide for 60 min at various temperatures (30, 50, 70, and 90 °C). Arrow indicates increasing temperature. Panels B and D represent the control experiment carried out without azide ion under identical conditions.

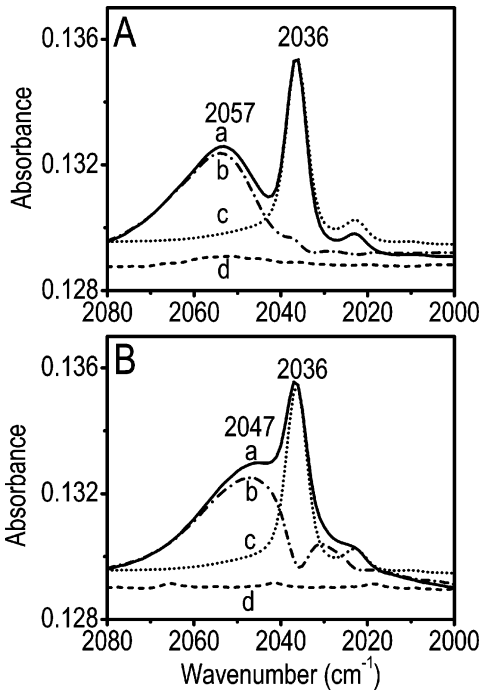

Figure 8. FTIR spectra of Au@Hem-N_3 (A) and Au@Cyt *c*-N_3 (B) recorded in KBr matrix. (A) Traces (a), (c), and (d) represent Au@Hem-N_3, Au@N_3, and Au@Hem. The trace (b) is obtained by subtracting (c) from (a). (B) Traces (a), (c), and (d) represent Au@Cyt *c*-N_3 prepared at 90 °C, Au@N_3 and Au@Cyt *c*. The trace (b) is obtained by subtracting (c) from (a). Au@Hem and Au@Cyt *c* are not showing any characteristic features in this region.

(40) Neya, S.; Chang, C. K.; Okuno, D.; Hoshino, T.; Hata, M.; Funasaki, N. *Inorg. Chem.* **2005**, *44*, 1193−1195.

(41) Bormett, R. W.; Asher, S. A.; Larkin, P. J.; Gustafson, W. G.; Ragunathan, N.; Freedman, T. B.; Nafie, L. A.; Balasubramanian, S.; Boxer, S. G.; Yu, N.-T.; Gersonde, K.; Noble, R. W.; Springer, B. A.; Sligar, S. G. *J. Am. Chem. Soc.* **1992**, *114*, 6864−6867.

(42) Miksa, D.; Brill, T. B. *J. Phys. Chem. A* **2003**, *107*, 3764−3768.

(43) Neya, S.; Tsubaki, M.; Hori, H.; Yonetani, T.; Funasaki, N. *Inorg. Chem.* **2001**, *40*, 1220−1225.

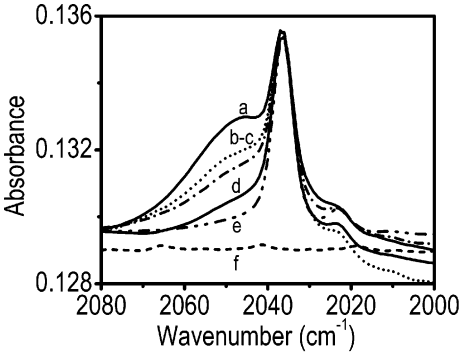

Figure 9. FTIR spectra of Au@Cyt *c*-N_3 prepared at (a) 90 °C, (b) 70 °C, (c) 50 °C, and (d) 30 °C. Traces (e) and (f) represent azide capped gold nanoparticles and Au@Cyt *c*, respectively.

The difference spectra (b) are obtained by subtracting trace (c) from trace (a). These give the $\nu_{as}(N_3)$-Fe(III) of Au@Cyt *c*-N_3 and Au@Hem-N_3 which are observed at 2047 and 2057 cm^{-1}, respectively. The difference in the vibrational frequency (10 cm^{-1}) between azide ion bound to the Hem and Cyt *c* can be attributed to penta and hexa coordinated Fe (III) centers, respectively.[43] As mentioned earlier in the mass spectra, the peak at *m/z* 681 in the LDI-TOF MS corresponds to the square pyramidal azide-hemin complex. The Fe (III) center of azide complex of a hemoprotien is hexa coordinated; the imidazole ligand is coordinated axially opposite to the azide ligand.[41]

The site of azide binding (nanoparticle and Fe (III) center) is affected by temperature. This was studied as described in the Experimental Section. In Figure 9, traces a−d represent the FTIR spectra of Au@Cyt *c*-N_3 prepared in aqueous phosphate buffered saline at different temperatures. There is a relative increase in the normalized intensity of the shoulder at 2047 cm^{-1} as a function of temperature. Although there can be other processes such as desorption of Cyt *c*, it is obvious that a greater fraction of azide ion binds to the Fe (III) center at higher temperature. High-temperature binding occurs in free Cyt *c* as well (see above). Unlike the Fe (III) center in Hem, the same in Cyt *c* is hindered by the axial imidazole ligands perpendicular to the porphyrin ring. Thus, the Fe (III) center of Cyt *c* is less accessible for the binding of azide, in comparison with Hem.

Summary and Conclusions

In this paper, we immobilized Hem (bovine) and Cyt *c* (horse heart) on the surface of Ag and Au nanoparicles. We have investigated the binding of a metabolic inhibitor azide ion to the active Fe (III) center of Hem and Cyt *c* bound to the nanoparticles using FTIR and Raman spectroscopies and LDI-TOF MS. The results show that the extent of reaction varies according to the geometry of heme containing molecule. The azide ion chemistry is similar to the parent unbound molecules. The study shows that nanoparticles act as excellent supports to perform the biochemical reactions and the course of chemistry can be probed in detail. The increased accessibility of the heme center at elevated temperatures make the azide ion bind the Fe (III) center preferentially. The difference in reactivity of Hem and Cyt *c* is attributed to their structural differences.

Acknowledgment. We thank the Department of Science and Technology, Government of India for constantly supporting our research program on nanomaterials. R.T.T. thanks Council of Scientific and Industrial Research (CSIR) for a senior research fellowship.

Supporting Information Available: Calculation of the surface coverage of the nanoparticles, LDI-TOF mass spectra of Ag@Hem and Ag@Hem-N_3, PSD mass spectra, TEM image and MALDI-TOF mass spectra of Au@Cyt *c*, fluorescence spectra of free Cyt *c*, Ag (II)@Cyt *c*, Ag (II)@Cyt *c*-N_3 and Au@Cyt *c* and FTIR spectrum of Ag@Cyt *c*-N_3. This material is available free of charge via the Internet at http://pubs.acs.org.

LA052035O